

Reactor design and operation strategies for a large-scale packed-bed CLC power plant with coal syngas

V. Spallina^a, P. Chiesa^{b,*}, E. Martelli^c, F. Gallucci^a, M.C. Romano^b, G. Lozza^b,
M. van Sint Annaland^a

^a Chemical Process Intensification, Chemical Engineering and Chemistry, Eindhoven University of Technology, Eindhoven, The Netherlands

^b Group of Energy Conversion Systems, Energy Department, Politecnico di Milano, Milano, Italy

^c Amec Foster Wheeler, Milan, Italy

Received 22 October 2014

Received in revised form 20 January 2015

Accepted 26 January 2015

Available online 4 March 2015

1. Introduction

The reduction of anthropogenic greenhouse gases emissions into the atmosphere in order to mitigate climate change is considered one of the major challenges for humanity (Metz, 2010). Carbon capture and sequestration (CCS) has been identified in recent decades as one of the most promising strategies to significantly reduce CO₂ emissions (up to 19% reduction according to IEA

(2014) especially from large-scale power production. Although CO₂ capture is feasible with different technologies, the main limitation for the industrial exploitation of CCS is the high efficiency penalty associated to CO₂ separation, purification and compression, and the increase in investment costs related to the large number of additional process equipment, in particular when using coal as primary fuel (Finkenrath, 2011; MIT, 2006). Among different technologies that have been discussed and presented, CLC (Fig. 1) represents one of the most viable solutions to achieve an effective mitigation of CO₂ emissions with a reduced efficiency penalty (Ishida and Jin, 1994). CLC occurs in the presence of a metal (called oxygen carriers, OC) which is oxidized in contact with air (Eq. (1)) and

* Corresponding author. Tel.: +39 0223993916.

E-mail address: paolo.chiesa@polimi.it (P. Chiesa).

Nomenclature

Symbols

B	stoichiometric coefficient for reaction of solid with reactant gas, mol _s /mol _g
Bi_m	biot number for the mass transfer
C_g	gas concentration, mol/m ³
C_p	heat capacity, J/kg K
C_s	solid concentration, mol/m ³
D_{ax}	axial dispersion, m ² /s
D_{eff}	effective diffusivity of gas mixture, m ² /s
d_p	particle diameter, m
E_{act}	activation energy, J/mol
h_m	element of mass transfer coefficient, m/s
k_{eff}	effective reaction constant = 1/s
k_g	pre-exponential factor = 1/s
L	reactor length, m
Mw	molecular weight, kg/kmol
Nu	Nusselt number
Pr	Prantl number
R	particle radius, m
r_g	grain radius, m
Re	Reynolds number
R_g	gas constant = 8.3144 J/(mol K)
rr	reaction rate, mol/m ³ s
Sc	Schmidt number
T	temperature, °C
t	time, s
t_{chr}	time controlled by chemical reaction, s
V	superficial gas velocity, m/s
X	solid conversion
Y	mass fraction, kg _i /kg _t
ΔH_R	reaction enthalpy, J/mol _i
Δp	pressure drop, %

Greek letters

ε_g	gas porosity
ε_s	solid porosity
ε_v	reactor void fraction
\emptyset	reactor internal diameter, m
Z	stoichiometric factor
η_v	effectiveness factor
λ_{ax}	effective heat dispersion (W/(m K))
M	absolute fluid viscosity, Pa s
\mathcal{E}	dimensionless radial coordinate in the particle = r/R
ξ_b	dimensionless position of boundary between reaction and diffusion zone in the particle = r_b/R
P	density, kg/m ³
ρ_m	molar density, mol/m ³
T	phase time, s
φ	sphericity
Φ	Thiele modulus

Abbreviations

ASU	air separation unit
CAPEX	capital expenditure
CCR	carbon capture rate
CCS	carbon capture and storage
CFBR	circulating fluidized bed reactor
CLC	chemical looping combustion
CPU	CO ₂ process unit
GT	gas turbine
HP/IP/LP	high/intermediate/low pressure
HRSG	heat recovery steam generator

HT/IT/LT	high/intermediate/low temperature
IGCC	integrated gasification combined cycle
OC	oxygen carrier
PBR	packed bed reactor
SMR	steam methane reforming
TIT	turbine inlet temperature
WGS	water gas shift

afterwards reduced (releasing the oxygen) in the presence of a reducing agent such as a fuel (Eq. (2) and/or Eq. (3)). The CO₂ contained in the exhaust gases from the reduction reaction is nitrogen-free and thus easily separated at high purity after water condensation. Many different oxygen carrier materials have been proposed and investigated for CLC operation (Adánez et al., 2004; Cho et al., 2004). From an energy point of view, the oxidation reaction is always exothermic and the O₂-depleted air is produced at high temperature, while the reduction reaction can be exothermic or endothermic depending both on the OC and on the fuel composition.



CLC has been successfully demonstrated in circulating fluidized bed reactors (CFBR) at atmospheric pressure from 500 W_{th} to 1 MW_{th} (Anheden et al., n.d.; Forero et al., 2009; Markström et al., 2013) and a 10 MW_{th} CLC loop is now under construction for a steam generation application (Sit et al., 2013). A wide discussion about recent progresses in chemical looping technologies is reported in the recent literature (Adanez et al., 2012; Hossain and de Lasa, 2008; Gallucci and van Sint Annaland, 2011).

As far as the application of CLC in large-scale power plants is concerned, different studies have been published in recent years mainly for pressurized CFBR operated with natural gas (Brandvoll and Bolland, 2004; Consonni et al., 2006; Naqvi and Bolland, 2007). The CO₂ capture rate (CCR) is in the range of 60–90% with an electrical efficiency between 43 and 52% power plant of hundreds of megawatt, depending on the configuration, assumptions and materials used. Recently, coal-fired power plants based on CLC systems have been discussed, generally starting from a sulphur-free syn-gas from a coal gasification unit as fuel for the CLC loop operated at high pressure (Cormos, 2010; Erlach et al., 2011; Sorgenfrei and

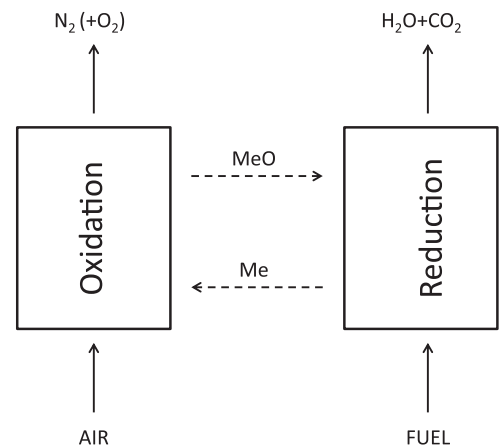


Fig. 1. Chemical looping combustion (CLC) concept.

Tsatsaronis, 2013). A CO₂ capture rate above 95% can be accomplished with an electric efficiency approaching 40%.¹

All these studies show that a high efficiency can be achieved when a CLC system replaces the combustor of a gas turbine included in a combined cycle. This requires the CLC reactors to be operated under pressurized conditions, which are extremely challenging to accommodate in circulating fluidized beds because high pressure makes the circulation of solids in a stable condition difficult. Due to gas turbine integration, the fluidized bed reactor must be operated at very high temperature (the higher the better in term of plant efficiency) and, as consequence, the oxygen carrier degradation becomes an important issue in terms of gas–solid reaction. Solids crushing due to attrition also worsen the separation of solids required before feeding the downstream gas turbine with the high temperature depleted air generated during the oxidation step.

An alternative for pressurized CLC applications using coal-derived syngas (or natural gas) are the dynamically operated packed-bed reactors, as the OC is not circulating and the gas is alternatively switched from the reactors (Noorman et al., 2007). The use of PBR for CLC is based on the different reaction and heat front velocities along the bed during a gas–solid reaction: during the oxidation phase, the gas–solid conversion proceeds very fast along the reactor, while the heat front velocity is significantly slower so that the heat of reaction is stored in the bed which is heated up to high temperature (i.e. up to more than 1200 °C depending on the OC and operating conditions). After the solids are completely converted, the heat can be removed from the bed (heat removal phase) by blowing additional gas which is released at high temperature and can be efficiently converted to mechanical power in a combined cycle. After the solids are completely oxidized (and the heat removed), the reactor is switched to reduction operation (reduction phase) and the solids are then reduced by converting the syngas into H₂O and CO₂. Intermittent purge phase is required to remove traces of reactant gases after the oxidation/reduction phases. The use of PBR for CLC has been presented and described with a detailed particle model integrated into a standard dispersion reactor model using CH₄ as fuel (Noorman et al., 2011a,b). The model has been validated with experimental results in a lab scale reactor (Noorman et al., 2010, 2011c) also using syngas from coal gasification (Hamers et al., 2014).

This work represents an original contribution to the development of large-scale power plant fuelled with syngas from coal gasification using PBR for CLC which is the main goal of the FP7 Democlock project. The reactor design, the system operation and their effect on the other components are assessed in order to estimate the plant investment, the resulting cost of CO₂ avoided and the competitiveness with alternative CCS technologies. Due to the low cost and thermo-mechanical properties (Ortiz et al., 2014) ilmenite has been selected as oxygen carriers. The present technology has not been studied yet for natural gas applications since other important issues, such as the low CH₄ conversion with ilmenite, which is also endothermic, makes the implementation challenging unless a different OC and heat management is not adopted. Following the heat management strategy described above, Hamers et al. (2013) proposed to use dual stage PBR system for CLC using Cu and Mn₃O₄ based OC, while a different approach for the heat management of a system operated with ilmenite (FeTiO₃) as OC has been discussed by the authors in a previous paper (Spallina et al., 2013). Although the use of PBRs for CLC is very promising for efficient fuel conversion with near zero CO₂ emissions, several problems have to be solved before industrial exploitation of this system can be considered: (i) the dynamic reactor operation that is characteristic of

packed-bed CLC can damage the turbomachines which cannot handle gas streams featuring rapid changes in temperature; (ii) the PBRs have to be assembled with a HT switching system (consisting of piping and valves) for which some technological issues need to be solved; (iii) due to the kinetics of the gas–solid reactions, the selection of the oxygen carrier type directly affects the heat management and therefore the system efficiency; (iv) the gas velocity has to be optimized considering a proper cycle time, acceptable pressure drop and mass and thermal dispersion.

The purpose of the present paper is the design of a network of PBRs for a real system operation for a hundreds-MW power plant working with syngas from coal gasification based on two different reactor configurations that have been optimized in a previous work (Spallina et al., 2014). The number and size of the reactors are strongly determined by the maximum pressure drop acceptable for the gas turbine. A sensitivity analysis relates the reactor geometry (i.e. diameter and length) as well as the particle properties and their influence in the gas–solid reactions. Afterward, a switching procedure is proposed for reactor operation in a full-scale power plant. Based on the heat/mass balances calculated for the full-scale power plants, the reactor behaviour has been investigated by means of a one-dimensional adiabatic model and used to obtain a detailed analysis of the entire system. Finally, the tuning of the dynamic operation of the PBR with the continuous operation in the other components of the plant is discussed.

2. System description

2.1. Heat management strategies

A detailed analysis of dynamically operated packed bed reactors for CLC has already been provided in Spallina et al. (2013) for a demo-scale plant using ilmenite as oxygen carrier and syngas from a coal gasification plant as fuel. A complete cycle consists of oxidation, reduction and heat removal phases. In the previous analysis two different reactor heat management strategies have been investigated which result from an optimization in terms of solid and fuel conversion and temperature control of the system. In the first case, the heat removal has been carried out by feeding air to the reactor after the oxidation phase until the bed is completely cooled down and, in the second case, inert gas (N₂) has been used in order to carry out the heat removal after the reduction cycle.

The second heat management strategy is based on the use of N₂ for the heat removal phase that takes place after the reduction phase in a bed with reduced solid material. In this case the reduction phase occurs directly after the oxidation phase (followed by a short purge) so that the solid material is at the maximum temperature and the syngas conversion is properly accomplished. Notably, this strategy proves effective just in case the oxygen carrier reduction is neutral or even exothermic so that the bed is maintained at the maximum temperature for the following heat removal stage. This is actually the case of reducing ilmenite with CO–H₂ syngas, (whose heat of reaction is weakly exothermic) considered in this study. Utilization of an abundant, cheap, non-toxic material such as ilmenite represents the relevant advantage offered by this strategy. On the other hand, this heat management strategy results ineffective for a combination of reducing agent and oxygen carrier leading to a strongly endothermic reaction (as it is the case of natural gas and ilmenite). In this case, the bed would significantly cool during the reduction phase resulting in an inefficient heat recovery during the following heat removal stage. For this strategy, two different configurations have been proposed:

- Co-current feeding (Fig. 2a): all the streams are fed from the same side of the reactor. Exhaust gases from the reactor operated in

¹ A recent study also discussed the possibility to convert pulverized coal directly in a CLC fuel reactor (Authier and Le Moullec, 2013).

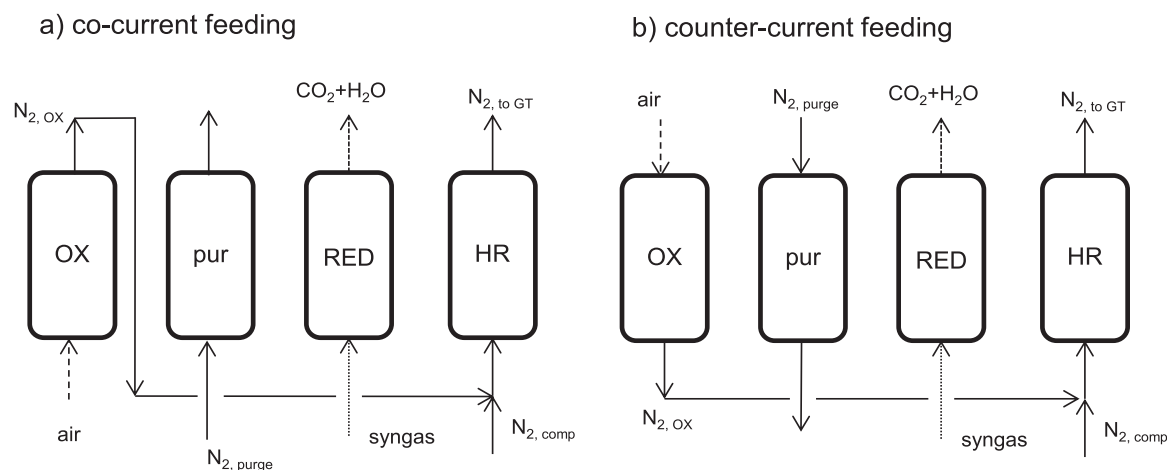


Fig. 2. Schematic of co-current and counter-current configurations discussed in (Spallina et al., 2013). OX = oxidation; pur = purge; RED = reduction; HR = heat removal.

reduction are produced mostly at high temperature. The exhaust conditions result from the bed temperature profile after the oxidation stage, because the high temperature solids at the end of the reactor heats up the CO_2/H_2O stream before it is discharged.

- Counter-current feeding (Fig. 2b): during oxidation and purge, the gas streams are fed at the opposite part of the beds with respect to the reduction phase. In this configuration, the CO_2/H_2O stream is produced at a lower average temperature, as a consequence of the bed temperature profile, whose left end side is at low temperature after oxidation and hence cools the reduction products at this temperature.

2.2. Main assumptions

The results from the heat management analysis proposed in our previous paper (Spallina et al., 2013) have been used to predict the mass and heat balances of a 450–500 MW_e 350–400 MW coal-fired power plant including a PBR based CLC system. The simplified layout of the plant considered in this work is reported in Fig. 3. The thermodynamic analysis, optimization and complete discussion of the plant integrated with PBR for CLC have been presented from the authors in Spallina et al. (2014) and the main data and assumptions resulting from the optimization are taken from that work. The coal is first converted in an oxygen-blown Shell gasifier using rich CO_2 in the lock hoppers to feed coal into the reactor. After the syngas coolers, the sulphur compounds present in the syngas are first converted into H_2S through a COS-hydrolysis fixed bed operated at 180 °C and then removed by means of a Selexol® absorption process using a mixture of dimethyl-ethers of polyethylene-glycol as solvent. The clean syngas is then mixed with recirculated exhaust gases leaving the reactor operated in reduction, in order to increase the oxygen content of the stream. The resulting stream is then preheated and finally fed to the packed bed reactor. The produced CO_2 -rich stream is cooled down to ambient temperature and, after the H_2O is separated by condensation, the residual CO_2 is dehydrated and compressed to 110 bar for the final storage. The oxidation phase is carried out by feeding air from an air compressor at 17 bar and the produced N_2 is then mixed with the N_2 main stream operating the heat removal phase. The gas turbine is designed as a semi-closed Joule–Brayton cycle where the N_2 required is compressed, heated up in the PBRs during the heat removal phase, expanded in a large-scale heavy-duty gas turbine and, after cooling in a heat recovery steam generator, part of it is vented to the stack and the remaining part is cooled to ambient temperature and recirculated at the compressor inlet. The CLC operating pressure has been set to a value (17) representing the

best compromise for the efficiency of the two configurations considered (co-current and counter-current feeding) as evidenced in Spallina et al. (2014). The negligible influence of the CLC operating pressure on the overall plant performance, fully justifies this assumption.

The PBRs are supposed to continuously process the mass flow rates of gases coming from the other sections of the power plant. A reactor network has been designed limiting the pressure drop over the reactors, because this strongly affects the plant performance. For a fixed reactor geometry and given solid material properties of the selected oxygen carrier, the pressure drop is mainly dependent on the gas flow rate, so that an increased number of reactors operated in parallel during the same phase are required to limit the pressure drop. This important effect implies that the reactor design and size assessment has to take into account the pressure drop associated to each single phase. For the present analysis, the maximum pressure drop has been set to 8%, as a design parameter which is of the main importance for the gas turbine. From a techno-economic point of view, the maximum pressure drop must be optimized: from one hand, by increasing the pressure drop a higher flow rate is handled by a single reactor reducing the cost of the CLC unit resulting in a lower capital cost. From the other hand, a higher pressure drop increases the air/ N_2 compressor power requirement thus reducing the overall plant performance and increasing the operational cost of the system. In the current authors' opinion, the assumed 8% pressure loss can be the optimal compromise between these conflicting requirements and it has been therefore adopted in this preliminary plant assessment. Other design constraints are dictated by the maximum size necessary to move pre-assembled reactors from a workshop to the plant at reasonable cost, and the minimum length according to a length-diameter ratio to ensure a homogeneous flow distribution over the entire reactor cross-section.

3. Reactor design

The assessment of the number of reactors has been carried out following the schematic procedure represented in Fig. 4. The calculation has been done for different reactor geometries by varying the internal diameter (\emptyset) and the reactor length (L). The solid material composition (inert to active OC ratio) has been chosen in order to reach 1200 °C during the oxidation phase (with a temperature increase of about 750–800 °C). A maximum admissible solid temperature of 1250 °C has been chosen in order to keep a safety margin to avoid local overheating and possible damage for the material despite the sintering temperature for ilmenite being 1595 °C.

In a fixed bed reactor the particle diameter is usually much bigger than in fluidized-bed reactors, because a relatively large

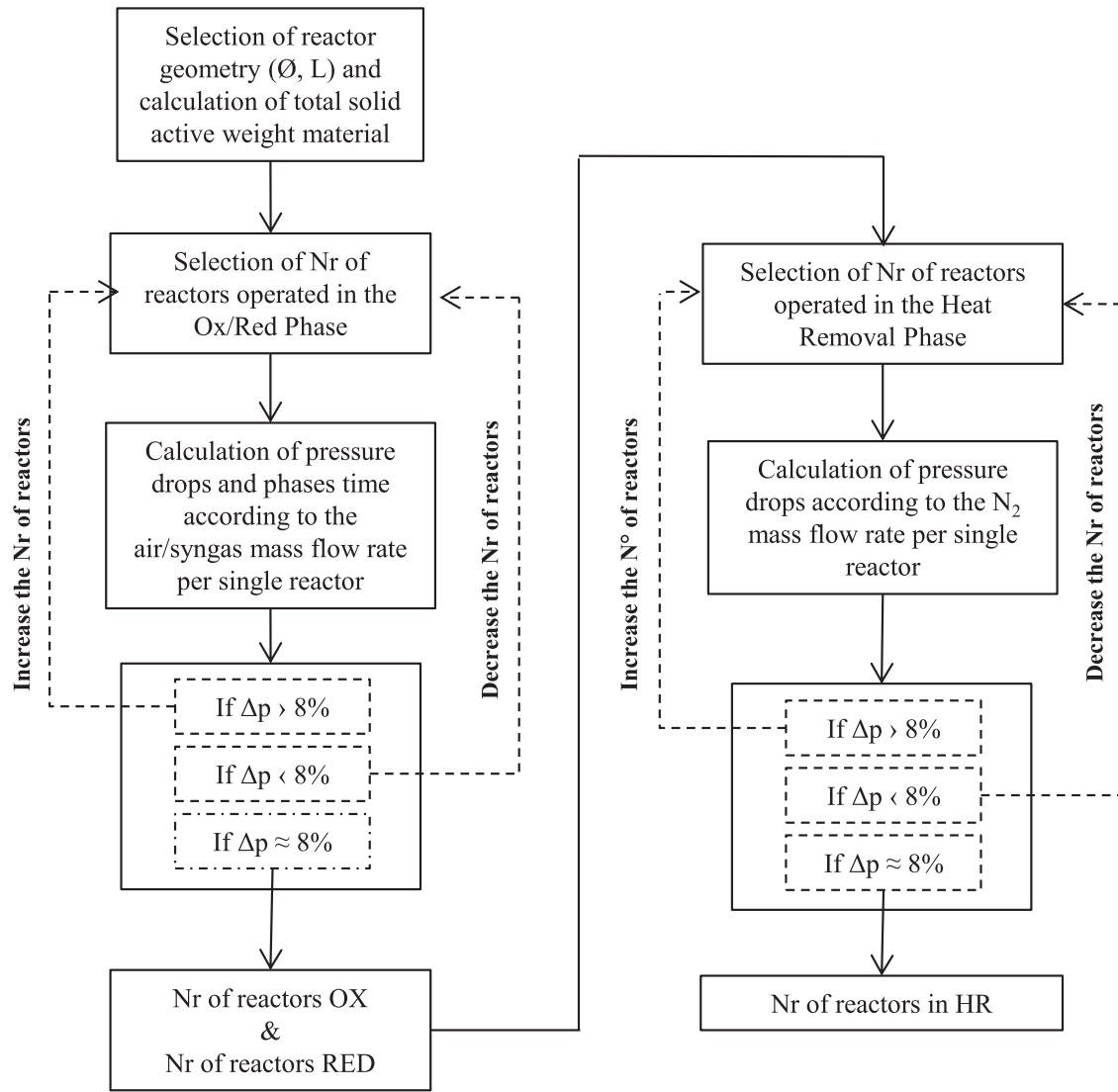


Fig. 4. Schematic of the procedure for the calculation of the required number of reactors.

particle diameter is required to limit the pressure drop, as easily deducible from Eq. (4). Fig. 6 presents the results of a sensitivity analysis on the total number of reactors carried out for a reactor of 5.5m diameter on the particle diameter by

changing the reactor length for both configurations considered. By increasing the particle diameter, the number of reactors drops significantly for both the co-current and counter-current configurations and the phase time is decreased from 17 min with d_p

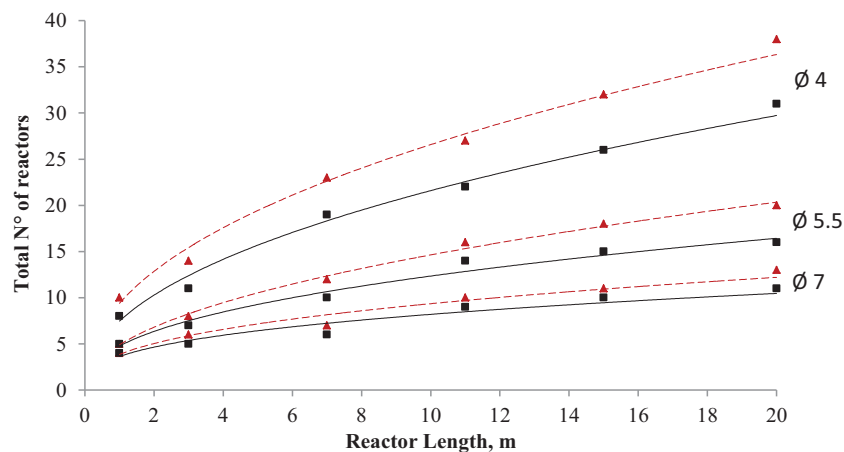


Fig. 5. Sensitivity analysis of the minimum number of reactors required for the co-current (■) and counter-current (▲) configurations for different reactor diameters (Ø) and lengths. The particle diameter is assumed 5 mm.

Table 1

Gas streams and solid conditions that have been used for the analysis of the two different configurations.

	Co-current	Counter-current
Air		
Total mass flow rate, kg/s		178
Pressure, bar		17
Inlet temperature, °C		404
Composition, %vol.	(0.92 Ar; 0.03 CO ₂ ; 1.03 H ₂ O; 77.28 N ₂ ; 20.73 O ₂)	
N₂ (HR + purge)		
Total mass flow rate, kg/s	577.5	797.7
Pressure, bar	17	17
Temperature, °C	437	437
Composition, %vol.	(1.16 Ar; 0.04 CO ₂ ; 1.31 H ₂ O; 97.5 N ₂)	
Syngas		
Total mass flow rate, kg/s		152
Pressure, bar		17
Temperature, °C		517
Composition, %vol.	(1 Ar; 33.6 CO; 34. CO ₂ ; 13.8 H ₂ ; 16.4 H ₂ O; 1.3 N ₂)	
Solid properties (oxidation/reduction)		
Active weight content, %wt.		30.6/32.9
TiO ₂ , content, %wt.		69.4/67.1
Solid porosity, %		40
Particle shape		Spheres
Main plant performance derived from (Spallina et al., 2014)		
Gas turbine, MW _e	168.9	224.6
Steam cycle, MW _e	238.2	182.1
Auxiliaries, MW _e	−60.9	−60.5
Net electric efficiency, %	40.55	40.50
CO ₂ emissions, kg/kWh _e	33.90	33.90

equal to 3 and 5 mm to almost 6 min in case of d_p equal to 20 mm.

This analysis assumes that the solid conversion is not affected by the particle size. However, a study (Noorman et al., 2011a) on a Cu-based oxygen carrier with a particle diameter equal to 1 mm showed that internal mass transfer limits the solid conversion already at this relatively small particle diameter. A numerical analysis (accomplished with the 1D particle model developed in Noorman et al. (2011a) and briefly discussed in the Appendix) has thus been carried out to quantify the effect of internal mass transfer limitations in our reactor. The volume of the spherical particle is kept constant and mass/density changes during the gas–solid reactions are accounted for in the porosity of the particle. The structure

of the particle is described by the porosity, the tortuosity and the average grain radius.

The particle model has been applied assuming four different particle diameters ranging from 1 mm up to 10 mm. Due to the strong dependence of the reaction rate on the temperature, the particle effectiveness factor has been estimated at different temperatures (as a function of the solid conversion). In fact, at higher temperatures the reaction kinetics is faster, so that the diffusion limitations become more prominent and the effectiveness factor decreases. In Fig. 7 are reported the solid conversion during the time at different d_p (left side) and the effectiveness factor profile at different temperature for the oxidation reaction (a) and the reduction with H₂ and CO (respectively b and c). The figures show that in case of CO this

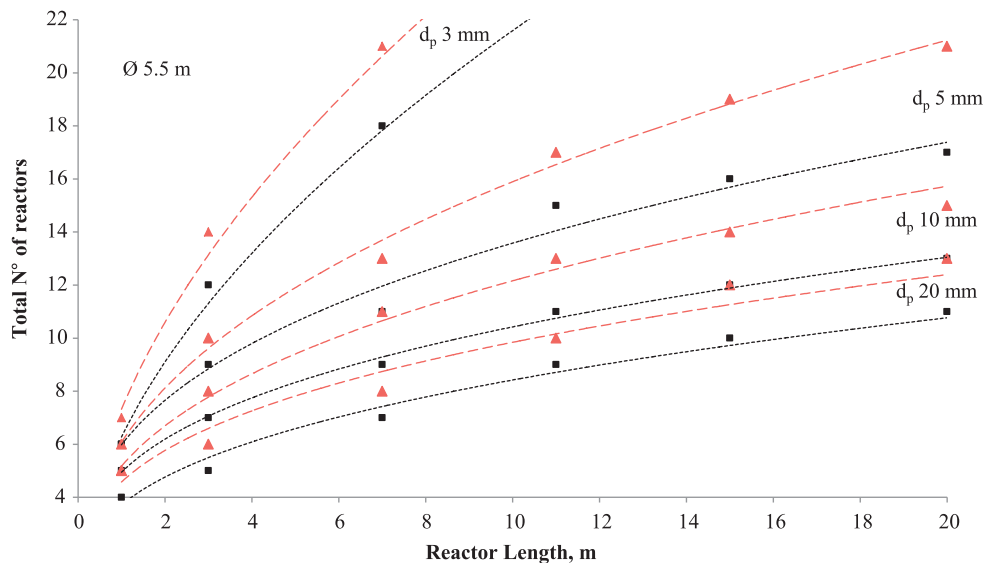


Fig. 6. Effect of the particle size on the total number of reactors required with an internal diameter equal to 5.5 m and different reactor lengths. Co-current configuration (■) and counter-current configuration (▲). The particle diameter is assumed 5 mm.

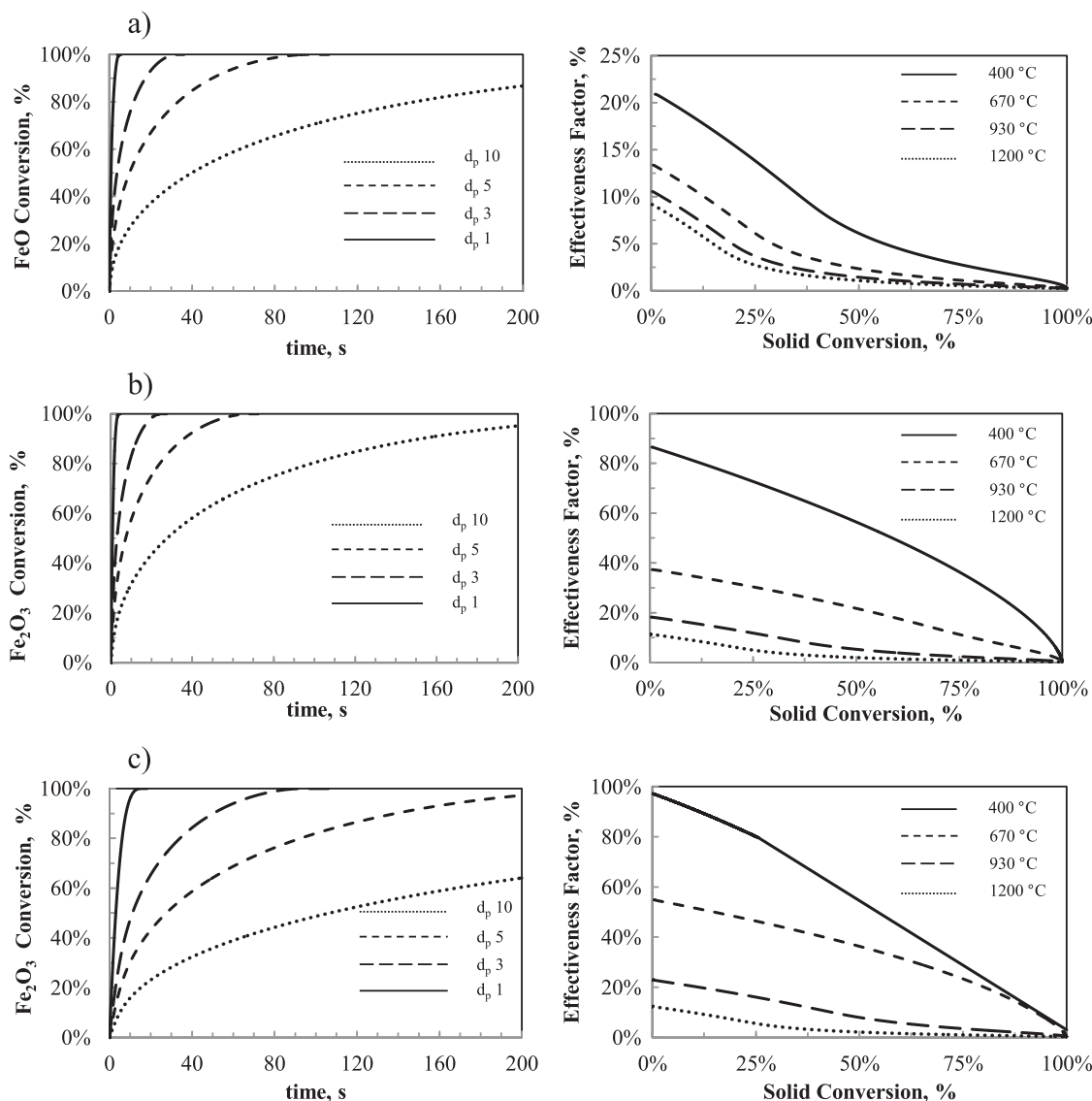


Fig. 7. (a) Oxidation is carried out with air (21% O_2 79% N_2); (b) reduction with H_2 (15% H_2 20% H_2O 65% N_2); (c) reduction with CO (15% CO 20% CO_2 65% N_2). On the left solid conversion occurs at 1200 °C with solid material with different particle diameter; on the right side the effectiveness factor depicted at different temperatures by varying the conversion of solid material with particle diameter of 5 mm.

effect is more pronounced due to the lower reactivity compared to the other reactions.

Despite the fact that selection of a larger particle diameter would significantly reduce the number of reactors required, its effect on the reaction rate is relevant. However, the model used for the assessment of the effectiveness factor has been validated with experimental data only at atmospheric pressure and thus some additional analysis is required for a more comprehensive description of the phenomena involved using high pressure CLC with large particle diameters. The heat management of the system discussed in the next paragraphs is referred to the 5 mm particle diameter. The corresponding effectiveness factors have been included in the kinetic model to calculate the solid conversion.

4. Operation strategy

The integration of dynamically operated PBRs in an IGCC power plant poses some significant challenges in terms of system operation. The IGCC plants are based on continuous operation and the turbomachines are designed to be properly operated in a limited

range of mass flow and temperature fluctuations. In the proposed system, the N_2 stream for the purge phase is taken from the main stream and used for the heat removal phase. The two streams are mixed together at the reactor outlet. The flow rate of the purge stream is set by assuming that an amount of N_2 equal to 5 times the reactor volume (required to effectively purge the reactor) is fluxed during a single phase time according to industrial practices.²

The operation strategy adopted has been selected to limit the flow rate, temperature and pressure fluctuations in the streams addressed to the plant components (especially the turbomachines) after the reactors in order to ensure safe operation.

No spare units are considered in the analysis. The sequences of the succeeding reactor phases are depicted in Fig. 8 for the co-current and counter-current configuration respectively. Note again that the different total number of reactors in the two different configurations results from the different N_2 mass flow rates required for the heat removal phase, as shown in Table 1.

² Ruben van Ruijven, Array Industries (personal communication).

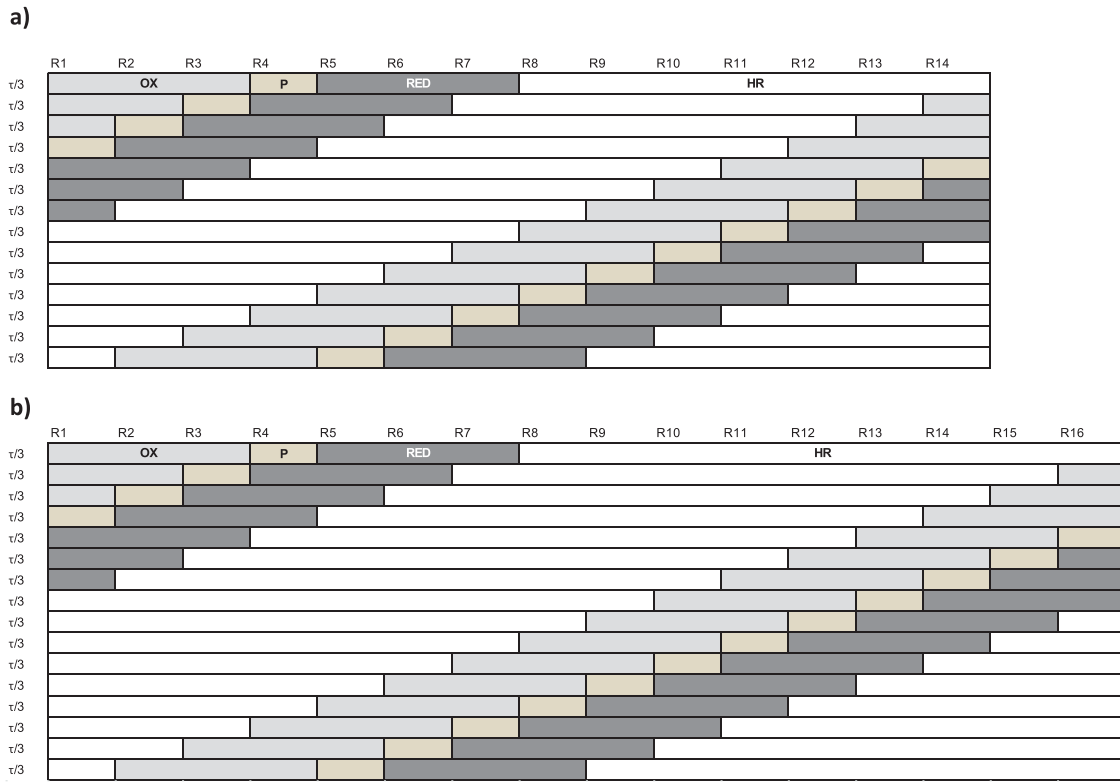


Fig. 8. Sequence of operation of the reactors during the cycle time in co-current (a) and counter-current (b) configurations. OX = oxidation; P = purge; RED = reduction; HR = heat removal.

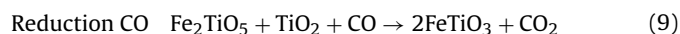
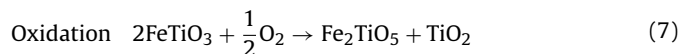
The sequence is based on running the reactors with a phase displacement of $1/3$ oxidation/reduction phase time (τ). This phase displacement allows one single reactor to be operated in the purge phase with a duration of $\tau/3$. The τ has been chosen equal to 90% of the time required to obtain full solid conversion to avoid excessive fuel slip during the reduction phase. The main results from the design procedure used as set values in the 1D adiabatic packed bed reactor model have been summarized in Table 2. From these results it is evident that the pressure loss governs the choice of the number of reactors in the heat removal phase, while the number of reactors in the oxidation/reduction phases is essentially determined by the assumed minimum phase time.

The benefits for turbomachines and heat exchangers downstream the CLC units due to a phase displacement for the reactor operation are shown in the next section.

5. 1-D analysis and reactor behaviour

5.1. Kinetic and thermal models

The model used for the present investigation is based on a 1D adiabatic axially dispersed packed bed reactor model, reported in the following sections. The kinetic model for the ilmenite conversion is based on equations provided by earlier work of Abad et al. (2011) and properly re-arranged (Eqs. (11–13)) to be used in the model. The gas–solid reactions for the oxidation and reduction cycle are:



$$\text{Reaction rate} \quad rr_i = (1 - \varepsilon_v)k_{eff}C_{g,i}^n \quad (10)$$

Derivation of k_{eff} from (Abad et al., 2011)

$$\frac{t}{t_{chr}} = 1 - (1 - X)^{1/3} \quad X = 1 - \left(1 - \frac{t}{t_{chr}}\right)^3 \quad (11)$$

Table 2

Summary of the results obtained from the design procedure.

	Co-current	Counter-current
Oxidation		
Internal diameter, m		5.5
Active reactor length, m		11
Particle diameter, mm		5
Reduction		
Specific inlet syngas flow rate, kg/(s m ²)	2.13	2.13
Number of reactors	3	3
Phase time, s	940	940
Pressure drop, bar	0.66	0.66
Pressure drop, % of p_{in}	3.9%	3.9%
Heat removal		
Specific N ₂ flow rate, kg/(s m ²)	3.29	3.36
Number of reactors	7	9
Phase time, s	2627	2816
Pressure drop, bar	1.05	1.3
Pressure drop, % of p_{in}	6.2%	7.7%
Purge		
Specific N ₂ flow rate, kg/(s m ²)	1.29	1.29
Number of reactors	1	1
Phase time, s	313	313
Pressure drop, bar	0.41	0.41
Pressure drop, % of p_{in}	2.4%	2.4%
Oxidation		
Specific inlet air flow rate, kg/(s m ²)	2.5	2.5
Number of reactors	3	3
Phase time, s	940	940
Pressure drop, bar	0.8	0.8
Pressure drop, % of p_{in}	4.7%	4.7%

$$\frac{dX}{dt} = \frac{3}{t_{chr}} \left(1 - \frac{t}{t_{chr}}\right)^2; \text{ if } t \rightarrow 0 \Rightarrow \frac{dX}{dt} \approx \frac{3}{t_{chr}}; \text{ where } t_{chr} = \frac{\rho_m r_g}{b k_s C_g^n}$$

$$\frac{dX}{dt} \Big|_{t \rightarrow 0} = \frac{3 \cdot b k_s C_g^n}{\rho_m r_g}; \text{ where } k_s = k_{so,i} \exp\left(\frac{-E_{act}}{RT}\right) \quad (12)$$

The total reduction of ilmenite to FeTiO₂ (Fe+TiO₂) has to be prevented because pure iron has low selectivity towards CO₂ and H₂O and working at high temperatures the solid tends to agglomerate into bigger Fe particles causing deactivation of the oxygen carrier as well as clogging of the packed bed. In this study it was assumed that the solid conversion does not include the intermediate solid states so that the active solid material goes from hematite (Fe₂O₃) to wüstite (Fe_{0.947}O), while titanium oxide is treated as inert material and does not take part in the chemical transformations. It must be noticed that also Fe₃O₄ appears during the reduction/oxidation reactions either as single component or in combination with TiO₂. In case of reduction from Fe₂O₃ to Fe₃O₄ the reaction rate is much faster than Fe₂O₃ to FeO (which is instead considered for this study) and therefore with a more completed kinetic model, part of the solid that will not react (as it is shown later because of low temperature) will be partly reduced from Fe₂O₃ to Fe₃O₄ with an increase in the oxygen transfer capacity of the bed. From a thermal point of view the temperature difference would be negligible due to the low heat of reaction associated. In case of oxidation, the reaction rate from FeO to Fe₂O₃ is already fast enough and therefore we do not expect any relevant change in the solid composition and in temperature profiles of the bed.

The main assumptions are: (i) radial temperature or concentration gradients are neglected³; (ii) the heat transfer limitations from gas to solid phase are accounted for in the effective heat dispersion (pseudo-homogeneous model); (iii) heat losses through the reactor wall are neglected. The governing equations of the mass and energy balances for the reactor model and the constitutive equations for the description of heat and mass dispersions are reported below. The numerical solution of the 1D reactor model is based on a finite difference discretization technique with higher order temporal and spatial discretization with local grid and time step adaption (Smit et al., 2005). More details about the reactor model can be found in Hamers et al. (2013) and Spallina et al. (2013) and the main equations are reported in the appendix (Eqs. (14–20)).

5.2. Model results

The dynamically operated PBRs have been simulated along a complete cycle (oxidation–purge–reduction–heat removal) with the operating conditions previously discussed. The results presented have been obtained after running the model about 10–15 cycles to reach cyclic steady-state conditions which represent the typical reactor behaviour.

5.2.1. Co-current system

The first simulation, related to the co-current configuration, has been run according to the operation strategy of Fig. 8a with the inlet conditions of the gas streams and the solid material properties shown in Table 1.

Fig. 9 shows the evolution of the gas temperature and the specific mass flow rates [kg_{gas}/(s m²)] at the reactor outlet of

a single reactor operated through subsequent oxidation/purge/reduction/heat removal phases in the cyclic steady state.

During the oxidation phase, the stream at the reactor outlet is composed of N₂ from ambient air completely deprived of oxygen except for the last fraction of the period when some oxygen is also detected, mostly caused by axial mass dispersion. During the reduction, the outlet gas mainly consists of CO₂ and H₂O and the mass flow rate increases due to the effect of the oxygen transfer. The fuel slip is detected at the end of the reduction phase where some unconverted CO and H₂ are released from the reactor. During the purge and the heat removal phases the N₂-rich streams do not change in concentration because only heat transfer occurs. Other species contained in the reactor at the beginning of the each phase are entrained with the stream. During the oxidation, N₂ is produced at different temperatures with a ΔT of about 450 °C. During the reduction phase, the exhaust gas temperature increases from 614 °C up to 1250 °C. The N₂ for the heat removal is leaving the reactor with a temperature that is decreasing from 1230 °C to 1070 °C. The temperature profile at the reactor outlet is determined by the solid temperature evolution profile during the cycle in the solid material (Fig. 10). After the heat removal phase (i.e. beginning of the oxidation phase) the solid temperature profile is around 450 °C in the first part of the reactor and in the last part the profile is not constant but a minimum solid temperature is present (around 340 °C); when the oxidation phase ends, the reaction front has reached the end of the reactor while the heat front has moved to the first 20% of the reactor length which is left at the inlet air temperature. At the end of the oxidation phase the maximum solid temperature is achieved (around 1200 °C), with a peak at 1270 °C in some restricted reactor zones (between the 75% and the 85%) where the solid temperature was about 500 °C at the beginning of the oxidation phase. After the purge phase the solid temperature profile along the reactor length does not change significantly (the heat front moves by about 2–3% of the total reactor length).

When the reduction starts the solid conversion occurs with two different conversion velocities: in the first part of the reactor the conversion proceeds slowly due to the local low temperature while the syngas is reacting very fast with solid material in the hot part of the reactor (Fig. 11). At the end of the reduction phase, the solid conversion is almost complete except for a small part at the beginning of the reactor. The solid temperature profile has changed (blue line in Fig. 10): the solid temperature drop to 330 °C is due because during the reduction the solid has been converted only by H₂ (the reduction of ilmenite with H₂ is endothermic). The reason for the solid temperature drop during the oxidation phase between the 30% and the 40% of the reactor length (see Fig. 10) is the small amount of unconverted solid during reduction between the 10% and the 20% of the reactor length in Fig. 11. Finally, during the heat removal phase, the bed is almost completely cooled down.

The results of the system operated with the conditions reported in Table 1 show two main problems: (i) the maximum solid temperature during the oxidation phase reaches 1270 °C in the second part of the reactor and (ii) the solid conversion during the reduction is low in the first part of the reactor which leads to a lower solid temperature (about 960 °C) in some restricted zones of the reactor after the oxidation reaction.

In order to keep the solid temperature below the assigned limit (1250 °C), a lower initial solid temperature has to be used (according to Eq. (5)) which directly depends on the inlet syngas temperature. Therefore by using 467 °C (instead of 517 °C) as inlet syngas temperature, the initial solid temperature decreases and after the HR phase the solid temperature profile is less fluctuating and the maximum temperature is limited to 1220 °C (Fig. 12).

³ This approach, introduced to avoid using time expensive 2D or 3D models, is justified in this specific case as radial gradient due to heat losses are moderated by the large size of the reactors. However, boundary effects due to variable temperature and concentration radial profile would lead to incomplete conversion in some part of the bed resulting in a lower utilization of the oxygen carrier (shorter phase time) and higher risk of fuel slip.

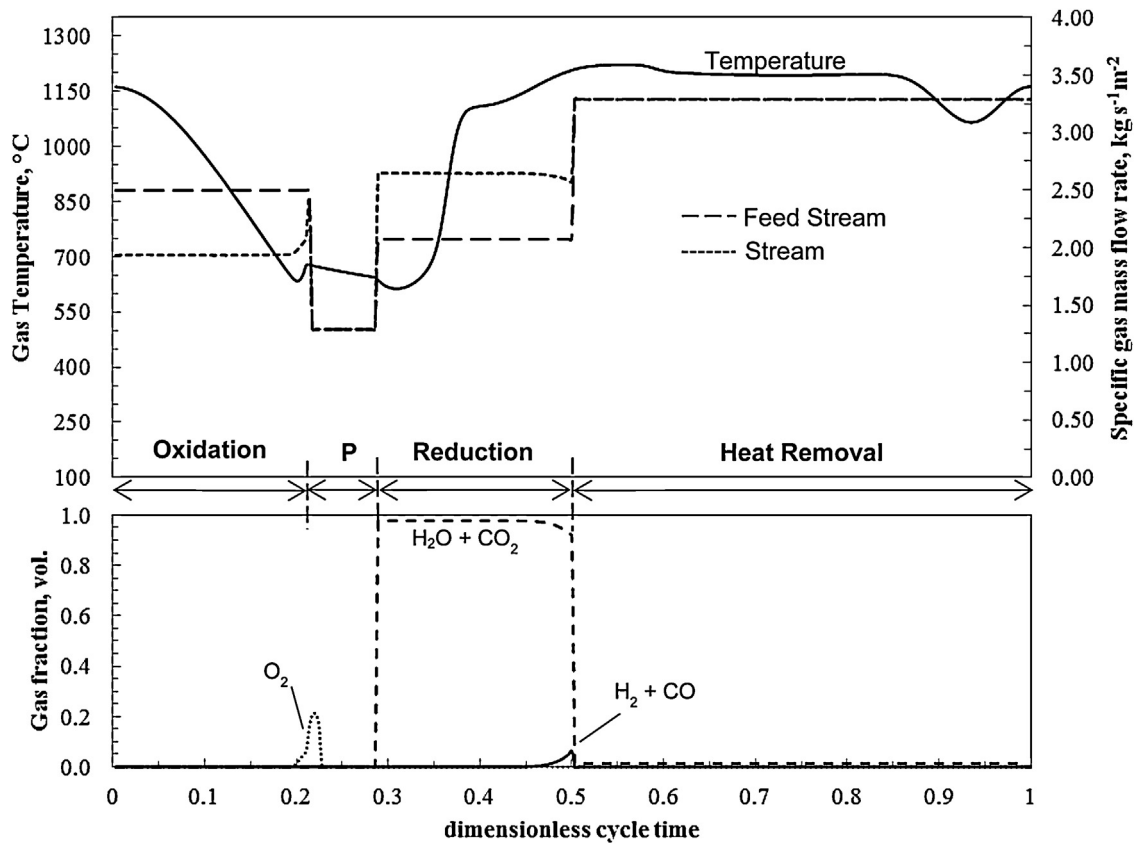


Fig. 9. Gas conditions (specific mass flow rate, temperature and species gas fraction) at the reactor outlet during a complete cycle in the co-current configuration.

For the complete solid during the reduction phase, a higher reaction temperature is required which implies a higher solid temperature especially in the part at lower temperature after the Oxidation phase (Fig. 12) and the initial solid temperature depends on the air inlet temperature. Almost complete solid conversion can be achieved if the air inlet temperature is increased (from 404 °C to 517 °C) because the syngas is reacting with the solid at higher temperatures in the initial part and therefore during the oxidation, all the reactor is reaching the maximum temperature (Fig. 12).

5.2.2. Counter-current system

The first simulation related to the counter-current configuration has been run with the gas inlet conditions and the solid material properties shown in Table 1, and the number of reactors calculated in Section 3.

Fig. 13a shows the stream outlet temperature and specific mass flow rates at the reactor inlet and outlet during the complete cycle. O₂ depleted air is released at constant temperature (about 440 °C) during the whole oxidation phase. When the bed is completely oxidized, the purge phase starts. Once the purge phase is completed,

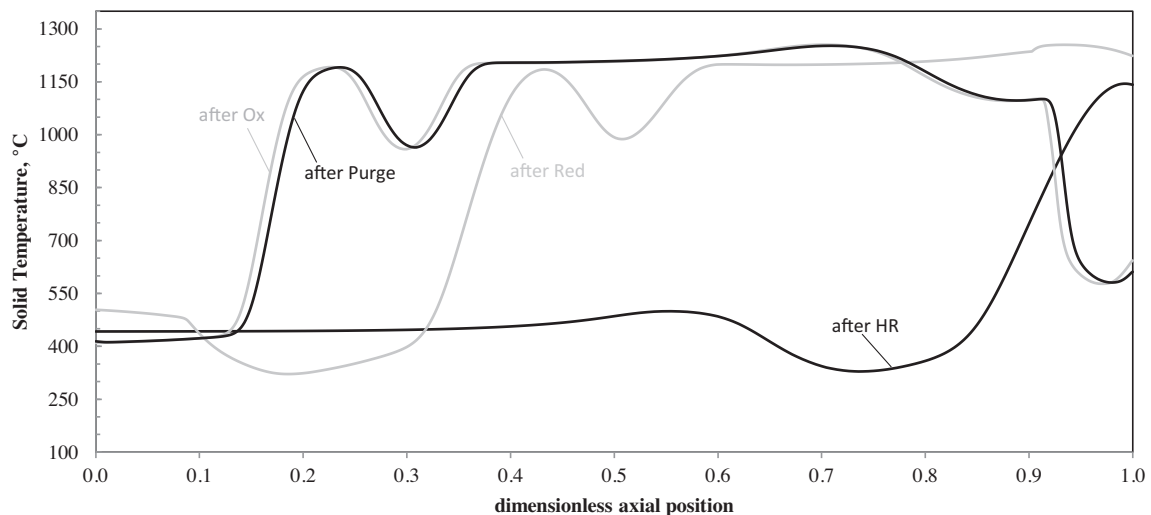


Fig. 10. Solid temperature profiles at the end of each of the phases for the co-current configuration. Inlet streams are fed at dimensionless axial position equal to 0.

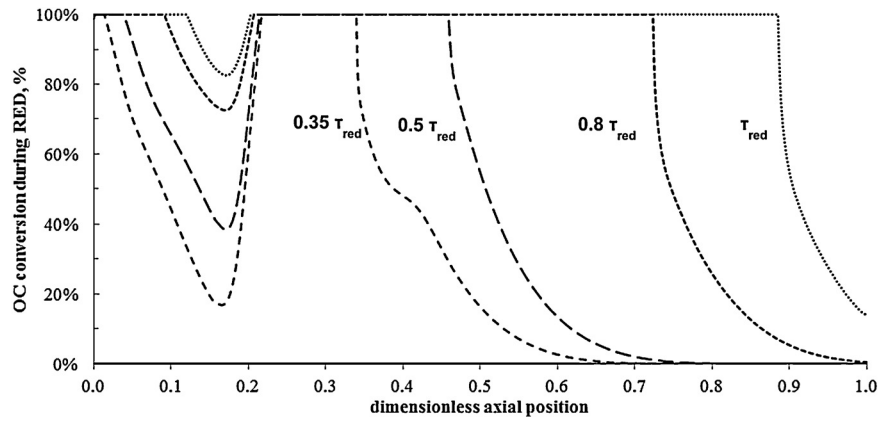


Fig. 11. OC conversion during the reduction phase for the co-current configuration.

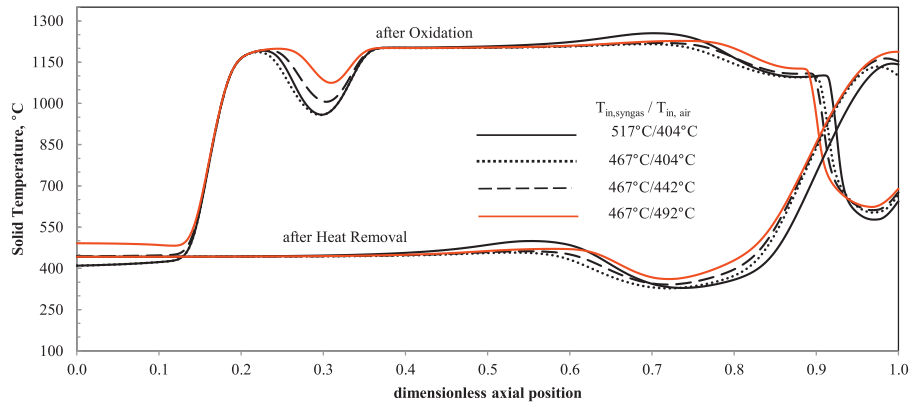


Fig. 12. Sensitivity analysis of inlet syngas and air temperature for the co-current configuration.

syngas is fed to the other reactor end (right hand side on the x-axis of Fig. 14) and the solid conversion proceeds very fast because the syngas is contacted with high temperature solids. The gas temperature at the reactor outlet increases up to 1275 °C at the end of the reduction phase. In the HR phase, after a long time in which N₂ is released at 1185 °C, the temperature drops to about 890 °C at the end of the cycle.

The temperature peak is due to an excessive overheating of the solids in the left hand side of the reactor (Fig. 13a) that occurs during the beginning of the oxidation phase when the OC is completely reduced and the initial solid temperature is high as can be deduced from Eq. (5). Reducing the temperature peak requires a slightly higher heat removal N₂ flow rate compared to the value selected for an 8% pressure loss. By increasing the specific N₂ mass flow rate from 3.6 to 3.8 kg/(s m²) the following trends can be discerned (Fig. 14):

- The OC conversion during the reduction phases decreases because the solid temperature on the left end of the reactor does not allow sufficiently fast kinetics and thus a higher fuel slip occurs. In fact, at lower specific N₂ flow rates, the OC on the left hand side of the reactor is always at the reduced state and never takes part in the reactions.
- As a consequence of the reduced solid conversion on the left end of the reactor during the reduction phase, the solid temperature after the oxidation phase presents a sort of dip which is more pronounced in the presence of a lower OC conversion.
- The slight increase in the N₂ stream during the heat removal phases (respectively 0.1 and 0.2 with respect to the initial 3.6 kg/(s m²)) implies that, for a given geometry of the reactors,

an equivalently higher N₂ flow rate has to be recirculated inside the gas cycle decreasing the average gas temperature from the reactors to the gas turbine and slightly increasing the pressure drop with a negligible effect on the overall plant efficiency.

- In case of abandoning a homogeneous active/inert material ratio distribution along the bed, the solid temperature profile could also be controlled and the temperature peak can be avoided by using the same gas flow rate in heat removal phase. However, this solution has not been investigated since the feasibility for a large-scale power plant is doubtful.

In terms of temperature fluctuations, the optimum solid temperature profile has been obtained for the N₂ mass flux of 3.7 kg/(s m²). The corresponding gas conditions at the reactor outlet during the complete cycle and the axial solid temperature profile along the reactor at the end of the cycle phases are depicted in Figs. 13b and 14. In comparison with the previously discussed co-current configuration (Fig. 9), the temperature profile at the reactor outlet during the reduction phase is less pronounced and there is no peak temperature during the heat removal phase; on the other hand more CO and H₂ is lost during the reduction phase because of fuel slip.

In Fig. 15 two main heat fronts can be distinguished: the first one moves from the right to left hand side of the reactor according to the feeding direction of the syngas and the N₂ for the heat removal phases and it is responsible for cooling down the part of the reactor already reduced. The second heat front moves from the left to the right hand side of the reactor following the feeding direction of the air (during oxidation) and the N₂ for the purge phase. During the reduction the heat front on the left side is moved back

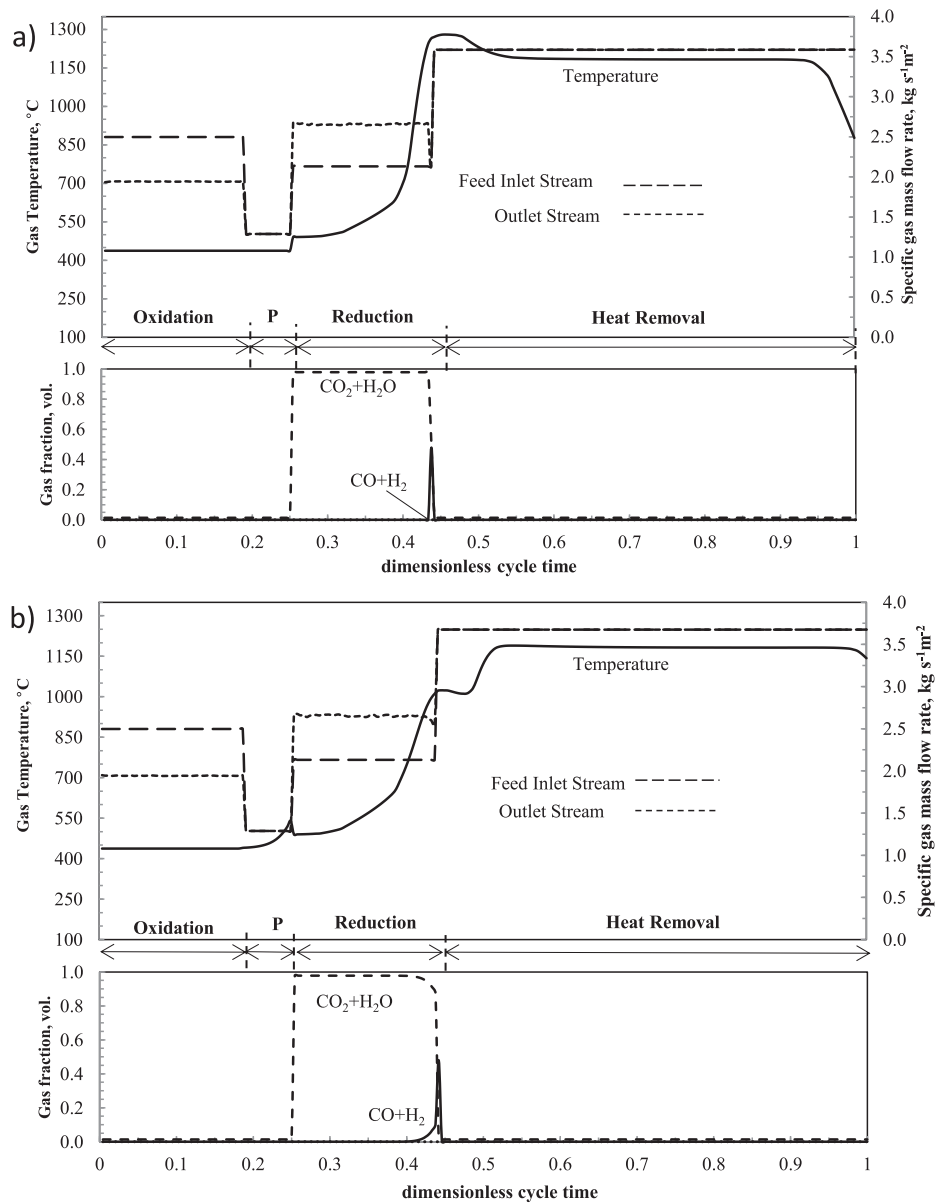


Fig. 13. Gas stream conditions (specific mass flow rate, temperature and species gas fraction) at the reactor outlet during a complete cycle for the counter-current configuration. (a) N_2 mass flux in the HR = $3.6 \text{ kg}/(\text{s m}^2)$; (b) N_2 mass flux in the HR = $3.7 \text{ kg}/(\text{s m}^2)$.

(from right to left) and the high temperature wave pre-heats the solid OCs before they are reached by the reaction front improving the kinetics. In fact, this configuration has the advantage that it keeps the high temperature heat coming from the oxidation reaction inside the reactor by moving it from right to left improving the solid conversion.

6. Dynamics of the CLC system during power plant operation

The results obtained from the dynamically operated PBR adiabatic model are finally used to define the conditions of the streams at the inlet of the gas turbine expander and the $\text{CO}_2/\text{H}_2\text{O}$ cooler placed after CLC block.

For the co-current configuration, the temperatures of the mixed gas streams leaving the reactors operated in the different phases are shown in Fig. 16a. Despite the exhaust gases leaving the single reactor with a maximum ΔT of 595°C (from 615°C to 1210°C) as shown

in Fig. 9, the heat exchanger downstream of the reactors operated in reduction receives a mixed gas stream with a maximum ΔT of 170°C (from 1020°C to 850°C) that is changing every $1/3 \tau$ (less than 6 min) according to the operation strategy proposed in Fig. 8. It may represent an important stream fluctuation for the steam generator, and therefore for the steam turbine, that should instead operate at stable conditions. However, the power plant is receiving additional steam from the syngas coolers and the heat recovery steam generator that mitigate those fluctuations. The O_2 -depleted air from the oxidation phase is released from a single reactor with a temperature fluctuation between 1160°C and 640°C . Due to the phase displacement in the reactor operation, the N_2 temperature fluctuation is significantly lower (close to 250°C) every $1/3 \tau$. The N_2 from the oxidation is then mixed with the N_2 that is compressed in the GT-compressor (which is almost 3 times higher than the N_2 leaving the reactor in oxidation) and a small fluctuation of 40°C occurs for the inlet flow during the HR phase. This fluctuation does not represent a problem for the reactor that is designed to handle a

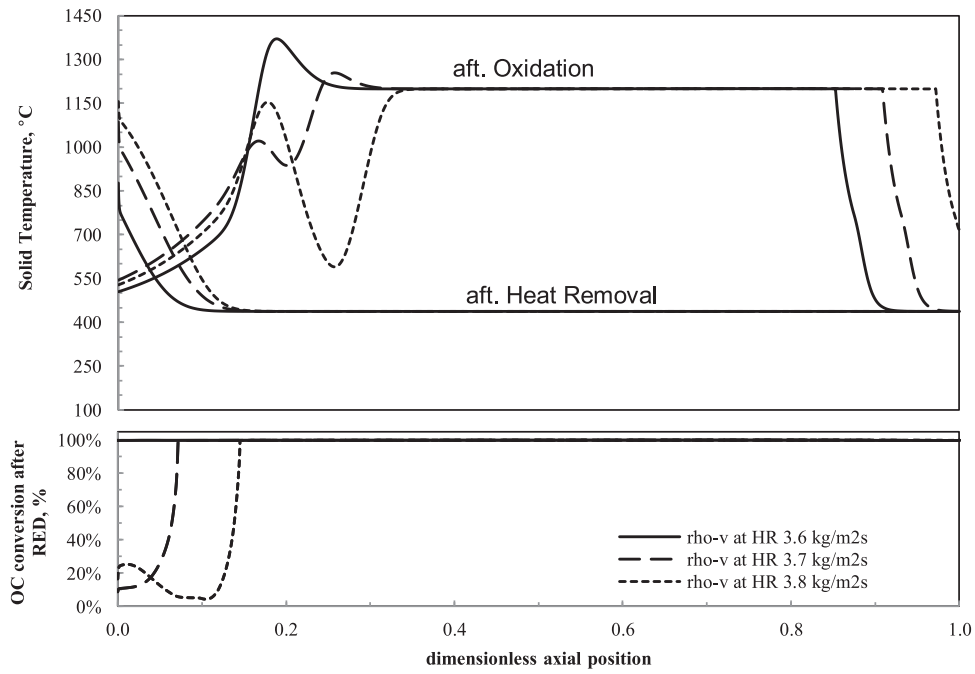


Fig. 14. Axial solid temperature profile after the oxidation and heat removal phases for different specific N_2 flow rates ($\rho\text{-}v$) during the HR.

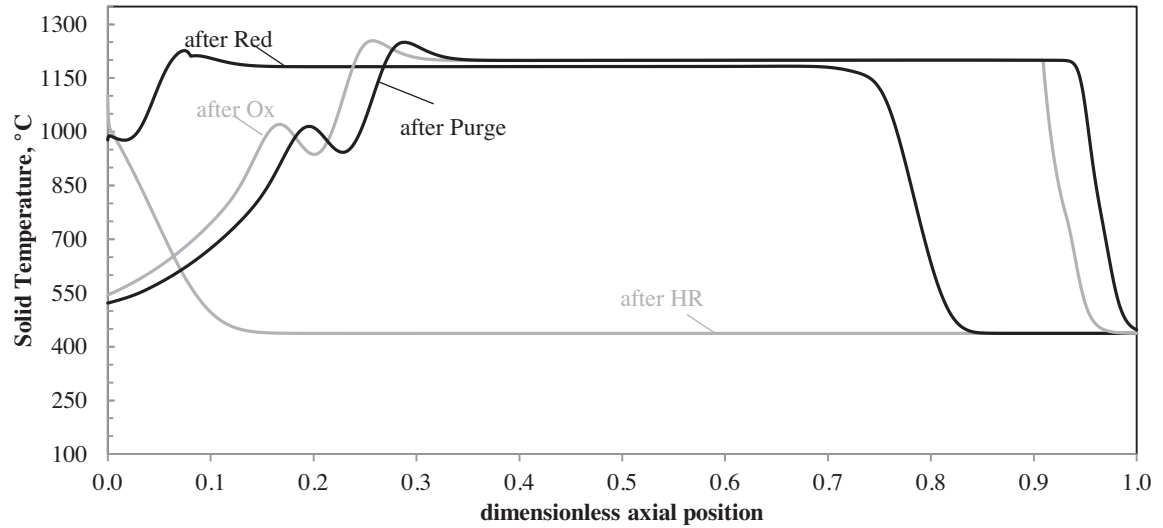


Fig. 15. Axial solid temperature profiles at the end of each of the phases for the counter-current configuration. Air and purge gas are fed from the left hand side, while syngas and N_2 for the heat removal are fed from the right hand side.

dynamic operation under very high temperature changes. Finally, during the HR phase, the N_2 is delivered from the single reactor from 1227 °C to 1132 °C but the mixed stream (from the 7 reactors operating with a phase displacement in heat removal) is sent to the GT with a small temperature change of 6 °C that is significantly lower than the maximum temperature fluctuation allowed for GT dynamic operation. It is important to notice that the temperature fluctuation occurs every time the reactors are switched (every $1/3 \tau$) which implies that also in the case of heat removal the temperature fluctuation frequency is independent of the number of reactors that are operated in parallel.

For the counter-current configuration, the gas conditions show different results (Fig. 16b). The exhaust gases from the reactor operated in reduction are sent to the cooling system with a temperature ranging from 544 °C to 713 °C which may require a specific design for the heat exchangers. The O_2 -depleted air is delivered from

the reactor at constant temperature (437 °C) which is the same as the N_2 stream that is delivered by the compressor. The maximum ΔT of the N_2 that is conveyed to the GT is around 6 °C, which is mostly due to the high temperature change of the N_2 during the HR (1011–1189 °C).

According to the results obtained in this paper the co-current configuration is more convenient because of the reduced investment costs associated with the CLC unit (due to the lower number of beds) without any relevant difference in the plant performance as shown in Table 1 and amply discussed in Spallina et al. (2014). Another important drawback for the counter-current configuration is the high sensitivity to the N_2 flow rate in terms of temperature control and solid conversion, as shown in Fig. 14, which make the system less flexible: conventional large-scale power plant usually are operated with different flow rates that depend on the dynamic of the turbomachines as well as the power production required.

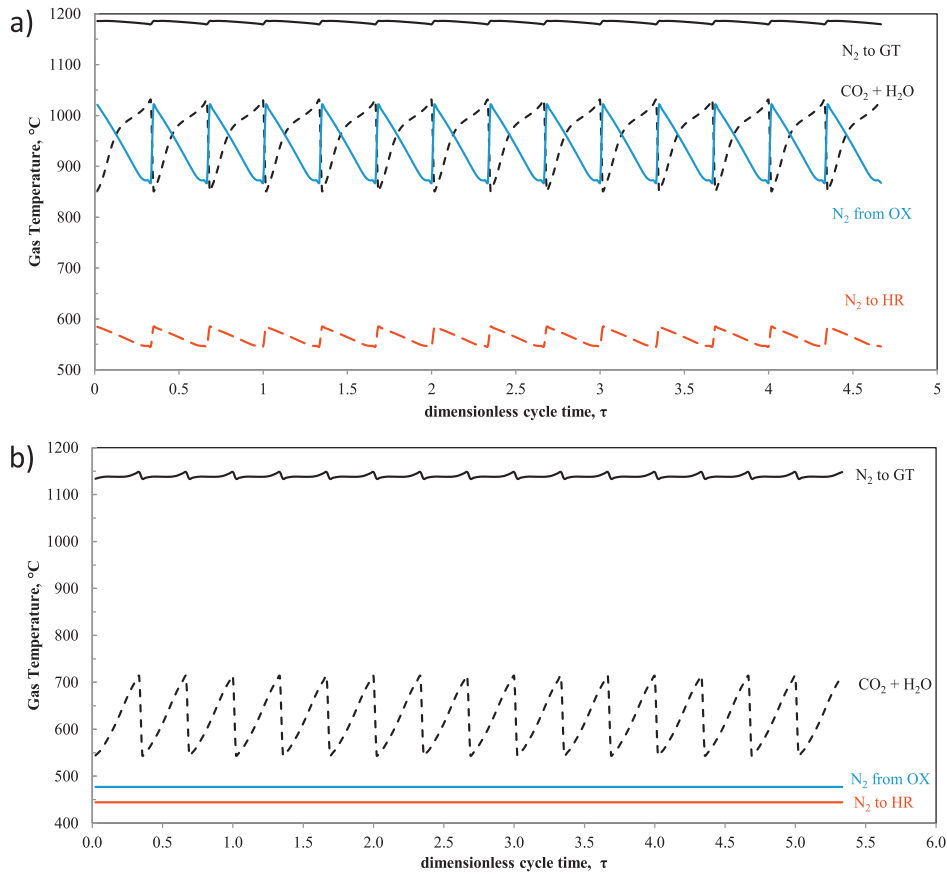


Fig. 16. Gas temperature after the mixing of the streams that are leaving the reactor operated in (a) co-current configuration ($T_{in,syngas}$ 466 °C; $T_{in,air}$ 520 °C) and (b) counter-current configuration (with 3.7 kg/m² s in the HR phase).

However, the co-current CLC PBR operation affects the power plant design in terms of gas turbine size, steam cycle complexity and cost of heat exchangers (especially in the case of co-current configuration for the exhaust cooling) and therefore a more detailed economic analysis is required. In this respect, assessment and design of the CLC units that have been discussed in this paper is essential in order to estimate the cost of the plant and the subsequent cost of electricity and CO₂ avoidance.

7. Conclusions

This paper has investigated the design and the heat management of PBRs for chemical looping combustion in a large-scale power plant operated with coal-derived syngas. The analysis was started with the calculation of the total number of reactors required to operate the plant in continuous mode. The reactor design assumptions imply that a short reactor length and a high diameter are preferable in order to reduce the number of reactor vessels (and thereby other critical components such as high temperature valves). The analysis has shown that 14–16 reactors (depending on the configuration adopted) with an internal diameter of 5.5 m and a length of 11 m are required for a fully integrated large-scale power plant. Adopting a 5 mm particle diameter (larger than the 3 mm considered in a previous analysis, (Spallina et al., 2013)), allows for reduction of the pressure losses and, consequently, the number of reactors, but some intra-particle diffusion limitations may prevail, lowering the solid conversion.

The possibility of switching the reactors with a proper phase displacement has been proposed for continuous plant operation

and has been discussed in detail. This method allows for reduction of the number of reactors by operating only one unit in purge and, most importantly, decreasing the temperature fluctuations of the gas streams sent to units downstream of the CLC system by properly mixing the gas streams exiting the reactors operated in parallel. A detailed analysis of the reactor behaviour employing an adiabatic reactor model has shown that the heat management strategies adopted for the configurations proposed are realistic. The CLC system releases a large N₂ flow at an adequately constant high temperature which can be conveniently used in a combined cycle for efficient power generation.

The effect of the inlet temperature of the syngas and air streams required for the co-current configuration was investigated to prevent overheating and ensure an almost complete conversion of the solids in the presence of a CO-rich gas like coal-derived syngas. As far as the counter-current configuration is concerned, it was concluded from the simulations that a precise selection of the specific velocity of the N₂ stream used in the HR phase is essential for a proper dynamic operation of the beds.

From an economic point of view, the use of PBR for CLC is directly related to the expected plant CAPEX cost due to the material required for the reactor construction and the amount of critical auxiliary components (such as HT valves and interconnecting piping), posing substantial limits to the feasibility of this technology. It is also important to highlight that the manufacture of specifically designed conventional equipment (i.e. turbomachines, heat exchangers, etc.) requires additional R&D costs that could significantly slow down the deployment of the technology. A more detailed economic assessment is required to balance these unfavourable aspects against the substantial advantages in plant

efficient permitted by the implementation of the PBR-CLC technology. The technical and economic implications of a full exploitation of PBR for CLC require additional research and investment, but based on the current study work, the technology proposed appears to lead to greater than 40% electric efficiency and reduced CO₂ emissions (the carbon capture rate is greater than 96%) which significantly reduce the costs associated with the implementation of CO₂ capture technology at large-scale in comparison with the benchmark technologies (pre-combustion plant can reach 35–37% of electric efficiency with CO₂ avoidance <90% as estimated in Spallina et al. (2014)). Moreover, a proper heat management and reactor design can reduce the gap between PBR which is at the early demonstration stage and the implementation of this technology at industrial scale.

Acknowledgements

The research leading to these results has received funding from the European Union Seventh Framework Programme (FP7/2007–2013) under grant agreement no. 268112 (Project acronym DEMOCLOCK).

Appendix

A.1. Particle model

The homogeneous model adopted (taken from Wen (1968)) is based on two stages of solid conversion: the first stage consists of a non-catalytic gas–solid reaction in which the solid on the external surface of the particle is converted by reacting with gas. The second stage starts when the material is completely converted on the external surface and the intra-particle diffusion limitations in the increasing product layer start to affect the average reaction rate so that a diffusion zone and a reaction zone are created respectively in the external and internal part of the particle. The model is used to estimate the effectiveness factor⁴ profile in the range of operating temperature and particle diameters in the analysis.

The solid conversion and the particle effectiveness factor are a function of the Thiele modulus⁵ (Φ) and the Biot number for mass transfer (Eqs. (21) and (22)). The main equations (Eqs. (23)–(25)) have been listed below. For a detailed description of the model the interested reader is referred to Noorman et al. (2011a):

$$k_{eff} \left[\frac{mol_g}{m^3_{particle}s} \right] = \frac{y_{i,act}^{OC,*} \cdot (\varepsilon_s \rho_{solid})}{Mw_{i,act}^{OC}} \frac{3 \cdot k_s}{\rho_m \cdot r_g} \cdot \eta_v^{**} \quad (13)$$

* where OC is FeO or Fe₂O₃ in $y_{i,act}$ and $Mw_{i,act}$ respectively for oxidation or reduction reaction; ** the effectiveness factor accounts for the change of the conversion during the time.

Gas phase balance

$$\varepsilon_g \rho_g \frac{\partial y_{g,i}}{\partial t} = -\rho_g v_g \frac{\partial y_{g,i}}{\partial x} + \frac{\partial}{\partial x} \rho_g D_{ax} \frac{\partial y_{g,i}}{\partial x} + \varepsilon_g r r_i M w_i \quad (14)$$

Solid phase balance

$$\varepsilon_g \rho_g \frac{\partial y_{g,i}}{\partial t} = -\rho_g v_g \frac{\partial y_{g,i}}{\partial x} + \frac{\partial}{\partial x} \rho_g D_{ax} \frac{\partial y_{g,i}}{\partial x} + \varepsilon_g r r_i M w_i \quad (15)$$

Energy balance

$$(\varepsilon_g \rho_g C_{p,g} + \varepsilon_s \rho_s C_{p,s}) \frac{\partial T}{\partial t} = -\rho_g v_g C_{p,g} \frac{\partial T}{\partial x} + \frac{\partial}{\partial x} \lambda_{ax} \frac{\partial T}{\partial x} + \varepsilon_g r r_i \Delta H_{R,i} \quad (16)$$

Effective axial heat dispersion

$$\lambda_{ax} = \lambda_{bed,0} + \frac{Re Pr \lambda_g}{Pe_{ax}} + \frac{Re^2 Pr^2 \lambda_g}{6(1 - \varepsilon_g) Nu} \quad (17)$$

from Vortmeyer and Berninger (1982)

$$\text{Heat Péclet axial number } Pe_{ax} = \frac{2(0.17 + 0.33 \exp[-24/Re])}{1 - (0.17 + 0.33 \exp[-24/Re])} \quad (18)$$

from Gunn and Misbah (1993).

$$\text{Nusselt number } Nu = (7 - 10\varepsilon_g + 5\varepsilon_g^2)(1 + 0.7Re^{0.2}Pr^{1/3}) + (1.33 - 2.4\varepsilon_g + 1.2\varepsilon_g^2)Re^{0.7}Pr^{1/3} \quad (19)$$

from Gunn (1978)

$$\text{Axial mass dispersion } D_{ax} = \left(\frac{0.73}{ReSc} + \frac{0.5}{\varepsilon_g + ((9.7\varepsilon_g^2)/ReSc)} \right) v_g d_p \quad (20)$$

from Edwards and Richardson (1968).

Biot number, Bi_m	$Bi_m = \frac{h_m d_d}{D_{eff}}$	(21)	
Thiele modulus, Φ	$\Phi = R \sqrt{\frac{\zeta k_g C_{s,0}}{D_{eff}}}$, D_{eff} is the effective diffusion coefficient accounting for Knudsen diffusion	(22)	
	First stage	Second stage	
Conversion X , %	$X = \frac{3}{\Phi^2} \left(\frac{\Phi}{\tan h(\Phi)} - 1 \right) \frac{\theta}{\theta_1}$	$X = 1 - \xi_b^3 + \frac{3\xi_b}{\Phi^2} \left(\frac{\Phi \xi_b}{\tan h(\Phi \xi_b)} - 1 \right)$	(23)
Effectiveness factor η_v , %	$\eta_v = \frac{3}{\Phi^2} \left(\frac{\Phi}{\tan h(\Phi)} - 1 \right) \frac{\theta}{\theta_1}$	$\eta_v = \frac{3}{\Phi^2 \xi_b^2} \left(\frac{\Phi \xi_b \cot h(\Phi \xi_b) - 1}{1 + \left(1 - \xi_b + \frac{2\xi_b}{Bi_m} \right) (\Phi \xi_b \cot h(\Phi \xi_b) - 1)} \right)$, where $x = r/R$	(24)
Dimensionless reaction time, $\vartheta_{1,2}$	$\theta_1 = 1 - \frac{2}{Bi_m} \left(\frac{\Phi}{\tan h(\Phi)} - 1 \right)$	$\theta_2 = 1 + \frac{\Phi^2}{6} \left(1 + \frac{4}{Bi_m} \right)$	(25)

⁴ The effectiveness factor is defined as the ratio between the actual overall rate of reaction and the rate of reaction that would result if the entire interior solid surface were exposed to the reactant gases at bulk conditions as: $\eta_v = \left(\left(\int_0^{r_b} r^2 \dot{m}_{g \rightarrow s}(r) dr \right) / \int_0^R r^2 \dot{m}_{g \rightarrow s, bulk}(r) dr \right)$ where r_b denotes the boundary between the diffusion and the reaction zones.

⁵ The Thiele modulus represents the ratio between the diffusion and the reaction time.

References

- Abad, A., Adánez, J., Cuadrat, A., García-Labiano, F., Gayán, P., de Diego, L., 2011. Kinetics of redox reactions of ilmenite for chemical-looping combustion. *Chem. Eng. Sci.* 66, 689–702.
- Adanez, J., Abad, A., Garcia-Labiano, F., Gayan, P., de Diego, L., 2012. Progress in chemical-looping combustion and reforming technologies. *Prog. Energy Combust. Sci.* 38, 215–282.
- Adánez, J., de Diego, L., Garcia-Labiano, F., Gayán, P., Abad, A., 2004. Selection of oxygen carriers for chemical-looping combustion. *Energy Fuels* 18, 371–377.
- Anheden, M., Fillman, B., Wolf, J., n.d. Parameter study in order to reveal critical design issues in the design for a CLC power plant using solid carbon as fuel. In: 1st International Conference on Chemical Looping, Lyon, France.
- Authier, O., Le Moullec, Y., 2013. Coal chemical-looping combustion for electricity generation: investigation for a 250 MW_e power plant. *Energy Procedia* 37, 588–597.
- Brandvoll, O., Bolland, O., 2004. Inherent CO₂ capture using chemical looping combustion in a natural gas fired power cycle. *J. Eng. Gas Turbines Power* 126, 316. Cho, P., Mattisson, T., Lyngfelt, A., 2004. Comparison of iron-, nickel-, copper- and manganese-based oxygen carriers for chemical-looping combustion. *Fuel* 83, 1215–1225.
- Consonni, S., Lozza, G., Pelliccia, G., Rossini, S., Saviano, F., 2006. Chemical-looping combustion for combined cycles with CO₂ capture. *J. Eng. Gas Turbines Power* 128, 525.
- Cormos, C., 2010. Evaluation of iron based chemical looping for hydrogen and electricity co-production by gasification process with carbon capture and storage. *Int. J. Hydrog. Energy* 35, 2278–2289.
- Edwards, M.F., Richardson, J.F., 1968. Gas dispersion in packed beds. *Chem. Eng. J.* 23, 109–123.
- Ergun, S., 1952. Fluid flow through packed columns. *Chem. Eng. Prog.* 48, 89–94.
- Erlach, B., Schmidt, M., Tsatsaronis, G., 2011. Comparison of carbon capture IGCC with pre-combustion decarbonisation and with chemical-looping combustion. *Energy* 36, 3804–3815.
- Finkenrath, M., 2011. Cost and Performance of Carbon Dioxide Capture from Power Generation.
- Forero, C.R., Gayán, P., de Diego, L.F., Abad, a., García-Labiano, F., Adánez, J., 2009. Syngas combustion in a 500 W_{th} chemical-looping combustion system using an impregnated Cu-based oxygen carrier. *Fuel Process. Technol.* 90, 1471–1479.
- Gallucci, F., van Sint Annaland, M., 2011. A review on recent patents on chemical and calcium looping processes. *Recent Patents Chem. Eng.* 4, 280–290.
- Gunn, D.J., 1978. Transfer of heat or mass to particles in fixed and fluidised beds. *Int. J. Heat Mass Transf.* 21, 467–476.
- Gunn, D.J., Misbah, M.A., 1993. Bayesian estimation of heat transport parameters in fixed beds. *Int. J. Heat Mass Transf.* 36, 2209–2221.
- Hamers, H.P., Gallucci, F., Cobden, P.D., Kimball, E., van Sint Annaland, M., 2013. A novel reactor configuration for packed bed chemical-looping combustion of syngas. *Int. J. Greenh. Gas Control* 16, 1–12.
- Hamers, H.P., Gallucci, F., Cobden, P.D., Kimball, E., van Sint Annaland, M., 2014. CLC in packed beds using syngas and CuO/Al₂O₃: model description and experimental validation. *Appl. Energy* 119, 163–172.
- Hossain, M.M., de Lasa, H.I., 2008. Chemical-looping combustion (CLC) for inherent separations—a review. *Chem. Eng. Sci.* 63, 4433–4451.
- IEA, 2014. CO₂ Emissions from Fuel Combustion.
- Ishida, M., Jin, H., 1994. A new advanced power-generation system using chemical-looping combustion. *Energy* 19, 415–422.
- Markström, P., Linderholm, C., Lyngfelt, A., 2013. Analytical model of gas conversion in a 100 kW chemical-looping combustor for solid fuels—comparison with operational results. *Chem. Eng. Sci.* 96, 131–141.
- Metz, B., 2010. Controlling Climate Change. Cambridge University Press, Cambridge, UK.
- MIT, 2006. The Future of Coal – An Interdisciplinary MIT Study.
- Naqvi, R., Bolland, O., 2007. Multi-stage chemical looping combustion (CLC) for combined cycles with CO₂ capture. *Int. J. Greenh. Gas Control* 1, 19–30. Noorman, S., Annaland, M.V.S., Kuipers, H., 2007. Packed bed reactor technology for chemical-looping combustion. *Ind. Eng. Chem. Res.* 46, 4212–4220. Noorman, S., Gallucci, F., van Sint Annaland, M., Kuipers, J.A.M., 2011a. A theoretical investigation of CLC in packed beds. Part 1: particle model. *Chem. Eng. J.* 167, 297–307.
- Noorman, S., Gallucci, F., van Sint Annaland, M., Kuipers, J.A.M., 2011b. A theoretical investigation of CLC in packed beds. Part 2: reactor model. *Chem. Eng. J.* 167, 369–376.
- Noorman, S., Gallucci, F., van Sint Annaland, M., Kuipers, J.A.M., 2011c. Experimental investigation of chemical-looping combustion in packed beds: a parametric study. *Ind. Eng. Chem. Res.* 50, 1968–1980.
- Noorman, S., Van Sint Annaland, M., Kuipers, J.A.M., 2010. Experimental validation of packed bed chemical-looping combustion. *Chem. Eng. Sci.* 65, 92–97.
- Ortiz, M., Gallucci, F., Snijders, F., Van Noyen, J., Louradour, E., Tournigant, D., van Sint Annaland, M., 2014. Development and testing of ilmenite granules for packed bed chemical-looping combustion. *Chem. Eng. J.* 245, 228–240.
- Sit, S., Reed, A., Hohenwarter, U., Horn, V., Marx, K., Proell, T., 2013. Cenovus 10 MW CLC field pilot. *Energy Procedia* 37, 671–676.
- Smit, J., van Sint Annaland, M., Kuipers, J.A.M., 2005. Grid adaptation with WENO schemes for non-uniform grids to solve convection-dominated partial differential equations. *Chem. Eng. Sci.* 60, 2609–2619.
- Sorgenfrei, M., Tsatsaronis, G., 2013. Design and evaluation of an IGCC power plant using iron-based syngas chemical-looping (SCL) combustion. *Appl. Energy* 113, 1958–1964.
- Spallina, V., Gallucci, F., Romano, M.C., Chiesa, P., Lozza, G., van Sint Annaland, M., 2013. Investigation of heat management for CLC of syngas in packed bed reactors. *Chem. Eng. J.* 225, 174–191.
- Spallina, V., Romano, M.C., Chiesa, P., Gallucci, F., van Sint Annaland, M., Lozza, G., 2014. Integration of coal gasification and packed bed CLC for high efficiency and near-zero emission power generation. *Int. J. Greenh. Gas Control* 27, 28–41.
- Vortmeyer, D., Berninger, R., 1982. Comments on the paper, theoretical prediction of effective heat transfer parameters in packed beds by Anthony Dixon and D.L. Cresswell. *AIChE J.* 28, 508–510.
- Wen, C.Y., 1968. Noncatalytic heterogeneous solid fluid reaction models. *Ind. Eng. Ind.* 60, 34–54.